Toxicology Research

PAPER

View Article Online
View Journal | View Issue

Cite this: *Toxicol. Res.*, 2016, **5**, 1078

An *in vitro* and *in vivo* bio-interaction responses and biosafety evaluation of novel Au–ZnTe core–shell nanoparticles†

R. Dunpall*[a,b] and N. Revaprasadu[b]

Received 1st February 2016,
Accepted 23rd April 2016

DOI: 10.1039/c6tx00054a

www.rsc.org/toxicology

Novel gold–zinc telluride (Au–ZnTe) core–shell nanoparticles were synthesized to support surface modifications for enhanced drug delivery in cancer therapeutics. Knowledge of the biosafety and biocompatibility properties of these materials within biological systems is very limited and needs to be evaluated before their potential bio-applications may be demonstrated. We report the *in vitro* and *in vivo* bio-interactions of the Au–ZnTe nanoparticles, which were exposed to various human cancer and healthy cells, an *in vitro* immune simulation using peripheral blood mononuclear cells, followed by the analysis of cytokine expression. Acute *in vivo* exposure studies using low (50 μg ml^{-1}), intermediate (500 μg ml^{-1}) and high (1500 μg ml^{-1}) concentrations of the Au–ZnTe particles were used to investigate histopathological effects in rats. Normal human mammary epithelial and colon cells in addition to human breast, prostate and colon cancer cells displayed cell viability between 86.4 ± 7.4% and 99.0 ± 3.6% when co-cultured with core–shell nanoparticles for 48 hours. Acute exposure studies using rat models displayed no significant changes in full blood counts, liver and kidney enzyme regulation and histopathology. These findings confirmed that Au–ZnTe core–shell nanoparticles display biosafety and biocompatibility features which can be exploited in future bio-applications.

Introduction

The synthesis and application of biocompatible nanoparticles with core–shell structures is rapidly gaining prominence across several disciplines within nanotechnology.[1] This trend has arisen because there is a growing need for new and versatile nanomaterials – exemplifying what has been called 'smart' architecture – with a growing suite of biological and chemical applications. Core–shell nanoparticles are synthesized by combining two or more different types of component materials. Such particles comprise a distinct core that is surrounded by a layer of 'shell' material.[2] Several types of core–shell nanomaterials exist, involving such combinations as semiconductor/semiconductor, magnetic/semiconductor and metal/semiconductor heterostructures.[2,3] The inherent optical, quantum confinement and electrical properties of the parent nanomaterials can be modified by the design and composition of the two-component materials.[3] For example, bio-imaging and photothermal therapy for localized destruction of tumour cells was recently illustrated using $Fe_3O_4/Cu_{2-x}S$ core–shell nanoparticles,[4] in which the Fe_3O_4 magnetic core was used as a contrast agent for magnetic resonance imaging whereas the $Cu_{2-x}S$ semiconductor shell converted absorbed near-infrared light energy into heat. The core–shell structure thus displayed enhanced and beneficial properties compared with its component parts.[4] In a recent study, Wang and co-workers were able to demonstrate the assembly of unique core–shell nanostructures composed by the surface modification of Fe and CoFe nanoparticles through doping with either zinc oxide or aluminum oxide to form core–shell nanoparticles that exhibit enhanced magnetic resonance imaging properties that could easily be utilized for improving tumour imaging applications.[5]

Core–shell nanoparticles comprising metal/semiconductor composites display a wide range of improved features due to the distinct interface regions characterised by the strong interactions between the metal plasmon and the semiconductor exciton (electron–hole pair). The objective of synthesizing metal/semiconductor core–shell nanoparticles is to control their shape, size, surface chemistry and optical stability. These types of nanoparticles have diverse properties and biocompatibility features that allow for the surface conjugation of biomolecules, chemotherapeutic drugs and cellular ligands. The parameters used to synthesize such nanoparticles for biologi-

[a]*Department of Biochemistry, University of Zululand, Private Bag X1001, Kwa-Dlangezwa, 3886, South Africa. E-mail: rekhadunpall@hotmail.com*
[b]*Department of Chemistry, University of Zululand, Private Bag X1001, Kwa Dlangezwa, 3886, South Africa*

†Electronic supplementary information (ESI) available. See DOI: 10.1039/c6tx00054a

cal applications involve precise optimisation of materials compatibility, temperature, pH, biocompatible surfactants and water solubility.[6] Sun *et al.*[7] describes a general high temperature method for the synthesis of water-dispersible gold metallic core surrounded by different transitional metal sulfide semiconductors (ZnS, CdS, AgS, NiS, and CuS). The gold–metal sulfide nanoparticles displayed enhanced optical and shape properties that can be utilized in plasmonics, and in optical applications.[7] Moreover, Lim and co-workers described the embedding of DNA within Au/Ag core–shell nanoparticles designed specifically for applications in biorecognition and optical stability studies.[8] Other research describes gold-coated iron oxide nanoparticles that are used as contrast agents in magnetic resonance imaging.[9] This study displayed the effect of combining two compatible types of nanomaterials that function as a single unit to enhance features such as size tunability as well as magnetic, optical and surface binding properties. In another study, Fe/Au core–shell nanoparticles were surface modified with anti-cancer drugs and used to increase drug release in cancer cells.[10] These findings demonstrate the versatility of gold-based core–shell nanomaterials in various bio-applications.[6–10] Researchers are currently focused on understanding the properties and surface chemistry features of these materials as much as demonstrating their potential applications.[11] Of particular interest to our research area are gold-based metallic/semiconductor core–shell nanomaterials.[1,12] We have recently reported the first synthesis of biocompatible cysteine-capped Au–ZnTe core–shell nanoparticles using a low thermal route.[13] The size range of the highly crystalline core–shell particles was 2–10 nm, which displayed uniform morphology and consistent optical properties. The *in vitro* cytotoxicity revealed on the basis of the WST-1 assay was studied on human pancreas carcinoma cell lines (PL45). Co-culture with Au–ZnTe nanoparticles displayed no adverse effects on the relative cell growth of these cells. In addition the cellular uptake and bio-imaging potential of the Au–ZnTe particles were demonstrated using transmission electron and fluorescence microscopy. The nanoparticles were observed to interact closely with the cell membrane, and confirmed the cellular uptake and isolation of Au–ZnTe nanoparticles within vacuoles. This interaction demonstrated the biocompatibility and functionality of using cysteine as a capping agent. In addition the Daphi filter set was used to validate the bio-imaging potential of these particular nanoparticles when co-cultured with PL45 cells.[13] This research has therefore not only highlighted the novelty and importance of the design and structure, but also described the physicochemical characteristics, of Au–ZnTe nanoparticles that appear to have the potential to facilitate their downstream application in drug delivery and bio-imaging.[13]

It is estimated that globally nanomaterials are produced in large quantities. However, because of toxicity, safety and hazard regulations only a small percentage of these materials end up in subsequent healthcare applications such as clinical trials, pharmaceutics and nanomedicine.[14–19] If they are to be used more widely, it is critical to establish their biosafety profiles across all platforms of research. The toxic responses to nanomaterial exposure have involved the evaluation of their effect on sub-cellular organelles and the correlation between *in vitro* and *in vivo* responses.[20] For example, Cui *et al.* illustrated the importance of the surface chemistry of nanomaterials and the role they play in bio-interactions with cells and other biological components.[21] The literature reports also that the cytotoxicity of nanomaterials can be attributed to a combination of factors such as morphology, composition and cell type.[22–25] Liu *et al.* investigated the *in vivo* toxicity of PEGylated FePt@Fe_2O_3 core–shell magnetic nanoparticles using various human cell lines and *in vivo* mouse models.[26] Their results demonstrated the importance of correlating various *in vitro* and *in vivo* experimental approaches to establish biosafety and toxicity on a relatively broad platform. *In vitro* biocompatibility studies of Au–Ag bimetallic alloy and core–shell nanoparticles were conducted using the survival rates of the microorganism *Daphnia magna* and showed their relevance across biological and environmental systems.[27] This work demonstrated the various *in vitro* approaches that may be used to determine the biosafety limits of heterostructured nanomaterials. A biosafety study generally aims to establish safe concentration/dose ranges that may be used in bio-applications such as drug delivery, bio-imaging, diagnostics and therapeutics,[28] across molecular, cellular, organ and integrated organs or whole animal systems.[29]

Initial reports on Au–ZnTe core–shell nanoparticles established their cytotoxicity and cellular uptake by human pancreas cancer cells. However, a fuller understanding of the potential interaction of these materials within more *in vitro* cellular and *in vivo* animal models is required, in which homeostasis, multiple cell cycle events, and organ responses are simultaneously investigated.[13] Thorough biosafety evaluation of *in vitro* experiments is currently limited to cell-cycle events and isolated cell culture studies, which permit comparison of different cell and tissue types. These studies provide the means to understand how nanomaterials interact with cellular organelles and biomolecules, thereby revealing information on mechanisms of cell death and pathway interactions.[29] Nanoparticles may enter biological systems through inhalation, dermal and ingestion routes, inevitably leading to bio-interactions with DNA, cells, tissues, organs and the blood circulation. The main objective of the study reported here was to evaluate for the first time the biocompatibility and biosafety effects of Au–ZnTe core–shell nanoparticles on human carcinoma and normal epithelial cell lines from different organs, their interaction with human peripheral blood mononuclear immune cells and to identify the clinical effects of their acute exposure in Sprague Dawley rats.

Experimental

Materials and methods

Compliance with ethical standards. This research was approved by the University of KwaZulu Natal (UKZN) Animal

Ethics Committee. All animal research was conducted at the Biomedical Resource Unit, UKZN, South Africa. Animal Ethics number: 085/14/Animal. The care and use of experimental animals in this study strictly complied with the approved University of KwaZulu-Natal animal welfare laws, guidelines and policies supported by the Research ethics committee and the National Society for the Prevention of Cruelty to Animals. The 3 R's and humane endpoint principles were followed in the design and implementation of the animal study. Access to veterinary care was ensured and available constantly by resident staff of the university's Biomedical Resource Unit.

Synthesis of Au–ZnTe core–shell nanoparticles. Au–ZnTe core–shell nanomaterials were synthesized using a previously reported one-pot solution method.[13] In a typical room temperature reaction, tellurium powder (0.041 g, 0.32 mmol) was mixed with sterile distilled water (15.0 ml) in a three-necked round-bottomed flask. A 15.0 ml aqueous solution of sodium borohydride (0.031 g, 0.79 mmol) was carefully added to the tellurium solution under inert conditions. After 2 hours of reduction, 20.0 ml aqueous solution of $ZnCl_2$ (0.0436 g, 0.32 mmol) and 40.0 ml aqueous solution of L-cysteine ethyl ester hydrochloride (0.1188 g, 0.32 mmol) were simultaneously added to the dark purple tellurium ion solution. The solution was stirred for 30 minutes followed by pH adjustment. The reaction was allowed to proceed at pH 7 for 3 hours at 60 °C. An aliquot of 40 ml of gold nanoparticle solution was added to the cysteine-capped ZnTe solution and the reaction was allowed to continue for 4 hours. The reaction mixture was filtered and centrifuged to give a dark, greenish black material that was readily dispersed in sterile distilled water and used for characterisation analysis.

Material characterisation of Au–ZnTe nanoparticles. A Perkin-Elmer Lamda 20 UV-vis spectrophotometer was used to monitor optical measurements in the 200–1100 nm wavelength range at room temperature. Samples were placed in quartz cuvettes (1 cm path length). Photoluminescence (PL) spectra were recorded on a Perkin-Elmer LS 55 luminescence spectrometer with xenon lamp over a range of 200–800 nm. The samples were placed in quartz cuvettes (1 cm path length) and the excitation peaks were recorded and analysed. Samples for scanning transmission electron microscopy (STEM) and transmission electron microscopy (TEM) imaging and spectroscopic analysis were prepared by drop casting an aliquot solution of the Au–ZnTe nanoparticles onto a TEM support grid (consisting of a holey carbon amorphous film supported on a copper mesh) and then allowing the solvent to evaporate at room temperature. Preliminary TEM imaging of the Au, ZnTe and the Au–ZnTe nanoparticles was performed using a Philips CM120 BIOTWIN instrument operated at 120 kV. A JEOL JEM 3010 URP high-resolution TEM (HRTEM) operated at 300 kV was used also for imaging of the Au–ZnTe samples. High angle annular dark field (HAADF) imaging was performed in a Titan G2 80-200 ChemiSTEMTM operated at 200 kV with a convergence angle of 18 mrad and HAADF inner angle of 54 mrad. TEM imaging of the cellular uptake of nanoparticles was performed using the Philips CM120 BIOTWIN instrument operated at 120 kV with the sample cooled to 80 K. The zeta potential was determined by dynamic light scattering using a Zetasizer (Malvern Nanoseries). Samples were filtered several times through a 0.22 mm millipore membrane filter prior to recording surface charge measurements.

Cell culture. Modified Eagle's medium (MEM), Ham's F-12K (Kaighn's) medium, McCoy's 5a medium, Dulbecco's phosphate buffered saline (PBS), trypsin, 100× pen-strep Fungizone and fetal calf serum were used for cell culture experiments. All the reagents were supplied by Whitehead Scientific. Human normal mammary breast epithelial (MCF12A), normal colon (CCD 841 CoN) and breast (MCF7), prostate (PC3), and colon colorectal (HT29) adenocarcinoma cell lines were purchased from American Type Culture Collection (ATCC) and used in the experiments. These adhesion cell lines were grown in appropriate culture media (MCF7, MCF12A, CCD 841 CoN-MEM, PC3-F12K, HT29-McCoy's 5a) containing 10% FBS and 1–2% PSF at a cell density of 5×10^5 cells per well. Cells that grew as monolayers were passaged, trypsinized and harvested for experimentation before reaching 100% confluency.

WST-1 cell viability assay. Cell viability was evaluated by WST-1 (4-[3-(4-iodophenyl)-2-(4-nitrophenyl)-2*H*-5-tetrazolio]-1,3-benzene disulfonate) assay (Roche Diagnostics, Mannheim, Germany) according to the manufacturer's instructions. Nanoparticle-treated and control cells were seeded in a 96-well plate at a cell density of 5000 per well in 100 μl of appropriate culture media. Cells were cultured in 5% CO_2 at 37 °C for 48 hours. Reconstituted WST-1 reagent was added to each treatment well and incubated for 2 hours at 37 °C. The plate was shaken for 30 seconds and the absorbance was measured at 450 nm using a Multiskan FC microplate reader. All experiments were repeated in triplicate and results are represented as mean ± standard deviation (SD).

Cellular interaction of Au–ZnTe core–shell nanoparticles. MCF7 cell lines were treated with Au–ZnTe core–shell nanoparticles for 48 hours at the following concentrations: 3.125, 6.25, 12.5, 25 and 50 μg ml^{-1}. The treated cells were then fixed with 2.5% glutaraldehyde for 24 hours, followed by a phosphate buffer wash. A postfix of 0.5% osmium tetroxide was added to the cells and incubated for 1 hour at room temperature, followed by a phosphate buffer wash. The cells were then dehydrated with 30, 50, 75 and 100% acetone. Resin and acetone were added to the sample in equal volumes followed by 4 hours' incubation at room temperature. Cells were placed in moulds and resin, followed by an overnight incubation at 70 °C. Resin sample blocks were sectioned into ultrathin cross sections using a microtome, stained and viewed in a TEM.

Human peripheral blood mononuclear cell culture. Human peripheral blood mononuclear cells (PBMCs) were isolated from donor blood samples obtained from the South African Blood bank. Density gradient centrifugation using Ficoll–Pague Plus method was used to isolate PBMCs from whole blood. The PBMCs were resuspended in RPMI-1640 cell culture media.

Alamar blue assay. The Alamar blue assay was used to evaluate the viability of PBMCs. These cells, at a density of 5000 cells per well, were seeded in a 96-well plate, where they were

stimulated with phytohemagglutinin (PHA). A control group of cells were not stimulated. After 4 hours of incubation with PHA, all cells were treated with Au–ZnTe nanoparticles in the following concentrations: 0, 0.09, 0.19, 0.39, 0.78, 1.5, 3.125, 6.25, 12.5, 25, 50 μg ml^{-1}. After 72 hours of exposure, 10 μl of alamar blue dye was added to each well and the absorbance was monitored at 570 nm using a Multiskan FC microplate reader. All experiments were run in triplicate and the results are represented as mean ± SEM.

Nanoparticle interference test. The optical interference of Au–ZnTe nanoparticles was evaluated to determine how Au–ZnTe nanoparticles interact with firstly the test reagent (WST-1 or resazurin from the alamar blue assay) in the absence of cellular and biological analytes and secondly how the nanoparticles interfere with the absorbance of the endpoint indicator product (formazan or resorufin). Au–ZnTe nanoparticles in the concentration range 20, 40, 60, 80 and 100 μg ml^{-1} was prepared and used in both interference tests. The first test was designed to evaluate the optical effects of Au–ZnTe nanoparticles with the cytotoxicity test reagents. Culture serum and WST-1 or alamar blue reagent was used as the controls. MEM culture media and different concentrations of nanoparticles was added to a 96 well plate (n = 4). The 96 well plates were then incubated for 48 hours for WST-1 and 72 hours for alamar blue in 5% CO_2 at 37 °C. After the incubation period 10 μl of either WST-1 or Alamar blue reagents was added to their respective plates and further incubated for 2 hours. Thereafter the plates were shaken for 30 seconds and the absorbance was measured at 450 nm and 570 nm for WST-1 and alamar blue respectively using a Multiskan FC microplate reader. The second interference test was designed to evaluate the optical effects of Au–ZnTe nanoparticles with the endpoint indicator or the reduced WTS-1/alamar blue reagents formazan or resorufin. For this test adherent MCF7 cells were seeded in a 96 well plate at a cell density of 4000 cells per well for WST-1 and suspension PBMC cells were seeded at a cell density of 5000 cells per well for alamar blue for 48 and 72 hours at 5% CO_2 at 37 °C. After the incubation period 10 μl of either WST-1 or alamar blue reagents were added into each well and further incubated for 2 hours (during this step live cells were able to convert or reduce the WST-1 or alamar blue reagent into formazan or resorufin). Thereafter the supernatant containing the formazan or resorufin was transferred into a new 96 well plate. The plate was shaken at 30 seconds and then read at 450 nm and 570 nm to determine the absorbance of the formazan or resorufin prior to their interaction with the nanoparticles. Nanoparticle concentrations ranging between 20 and 100 μg ml^{-1} was then added into respective wells and the absorbance was recorded to establish any interference effects of Au–ZnTe nanoparticles with formazan and resorufin.

Cytokine analysis. The concentrations of proinflammatory cytokines, tumour necrosis factor (TNFα), interferon (IFNγ) and interleukin (IL-1β) from phytohemagglutinin-stimulated and non-stimulated PBMCs were measured using a BD Bioscience ELISA kit. Each well was coated with 100 μl of capture antibody and incubated overnight at 4 °C. PBMC fluid serum was added to each well after washing and blocking with assay diluent. Cytokine-containing culture media and cytokine standards were added to each well and incubated at room temperature for 2 hours. After washing, the respective detection antibody was added to each well and incubated at room temperature for 1 hour. Plates were washed again and incubated with Avidin-Horseradish peroxidase for 30 min, followed by detection with tetramethylbenzidine solution. The reaction was stopped by the addition of H_2PO_4 and the absorbance was measured at 450 nm using a Multiskan FC microplate reader. All experiments were conducted in quadruplicate and are represented as mean ± SD. The cytokine concentrations were calculated from a standard curve (range: 10–1000 pg ml^{-1}) derived from cytokine standards available with the BD Bioscience ELISA kits.

Animals and conditions. Four-week-old female, specific-pathogen-free (SPF) Sprague Dawley rats were from the Biomedical Resource Unit, University of KwaZulu-Natal and acclimated for 7 days before starting the experiments. During the acclimation and experimental periods, the rats were housed in polycarbonate cages (maximum of 3 rats per cage) in a room with controlled temperature (22.2 ± 1.7 °C) and humidity (48.4 ± 6.0%), and a 12 h light/dark cycle. The rats were fed a rodent pellet food and water *ad libitum*. Au–ZnTe core–shell nanoparticles were filtered, weighed, resuspended in PBS and prepared for administration to the rats by intraperitoneal (IP) injection. The animals were divided into 4 groups of 3 animals each: untreated control (PBS only), low-dose group (50 μg ml^{-1}), intermediate-dose group (500 μg ml^{-1}) and high-dose group (1500 μg ml^{-1}). After the acclimatization period, a volume of 0.5 ml Au–ZnTe nanoparticles was administered to the rats *via* IP injection. Animals were then placed individually in metabolic cages for 24 hours for observation and urine analysis using commercial urine dipsticks.

Biochemical evaluation of liver and kidney function. Food was withheld for 12 hours before necropsy at the conclusion of the 14 day acute toxicity study. On day 14 the animals were anesthetised by an overdose of halothane followed by immediate bleeding and exsanguination by cardiac puncture. The blood was collected in heparinized vacutainers, and analysed for alkaline phosphatase (ALK Phos), alanine aminotransferase (ALT), gamma-glutamyl transpeptidase (gamma-GT), lactate dehydrogenase (LDH), creatinine (CRE) and urea using a Beckman Coulter DXC600/800 instrument. The counts of white blood cells (WBCs), red blood cells (RBCs), and of platelets (PLT) were recorded using a Roche Sysmex XT1800.

Histopathology analysis of liver and kidney tissue. The kidney and liver organs were carefully harvested, weighed and fixed in a 10% formalin solution containing neutral PBS. For light microscopy (LM) examination, the tissue samples were removed from the fixative and dehydrated using a 50–96% ethanol gradient with the ethanol being subsequently cleared from the tissue using xylene. The tissue was then embedded in paraffin wax using standard procedures. The wax-embedded tissue was sliced into 3 μm sections using a microtome, col-

lected on glass slides, dried and stained with hematoxylin and eosin (H&E) using standard protocols. The stained sections were examined using a light microscope (Nikon 80i, Kanagawa, Japan) and images were digitally captured using NIS Elements D software and a camera (Nikon U2). All experiments/evaluations were performed using a minimum of three replicates.

Statistical analyses. The statistical analyses were performed using GraphPad Prism® Version 5 software. The statistical evaluation included one-way analysis of variance (ANOVA) followed by Kruskal–Wallis test or a two-tailed Student's *t*-test followed by Mann Whitney test. The level of statistical significance was set at $p < 0.05$.

Results

Synthesis and characterisation of Au–ZnTe core–shell nanoparticles

The core–shell nanoparticles were synthesized under inert atmospheric conditions using a novel one-pot method.[13] After 2 hours, a dark purple colour was observed to indicate the reduction of tellurium powder in the reaction. The addition of zinc chloride and L-cysteine ethyl ester hydrochloride (surface capping agent) was added to the reduced tellurium and produced a dark brown solution. The material obtained from this reaction was purified using sterile filtering techniques for morphology, surface chemistry and optical analysis (Fig. 1A).

The morphology of the nanoparticles was studied using atomic force, transmission electron and high-resolution transmission electron microscopy. Uniform spherical morphology was observed (Fig. 1B, E and F). The average particle size was observed as 7 ± 3.74 nm (Fig. 1C). The nanoparticles displayed crystalline properties and a lattice spacing of 0.34 nm was calculated from high-resolution TEM micrographs (Fig. 1D).

Micrographs observed using elemental mapping by X-ray energy dispersive spectroscopy (XEDS) in the STEM supports a core–shell morphology; the results shown in Fig. 2A–D confirm the presence of Zn and Te elements distributed around the Au core. Line scans showed that the thickness of the ZnTe shell varied considerably between different regions of the sample.

The absorption properties of the core–shell material was measured at 538 nm (Fig. 3A), displaying a small red shift

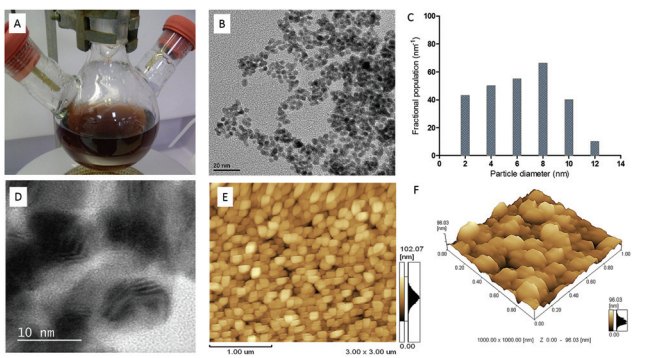

Fig. 1 Morphological characterisation of Au–ZnTe core–shell nanoparticles. (A) A solution of Au–ZnTe nanomaterial. (B) TEM image of particle size and shape. (C) Size distribution of Au–ZnTe core–shell nanoparticles. (D) HRTEM evaluation showing lattice fringes. (E) AFM 2-D evaluation showing uniform distribution of nanoparticle size and shape. (F). AFM 3-D analysis showing uniform surface features of Au–ZnTe core–shell nanoparticles.

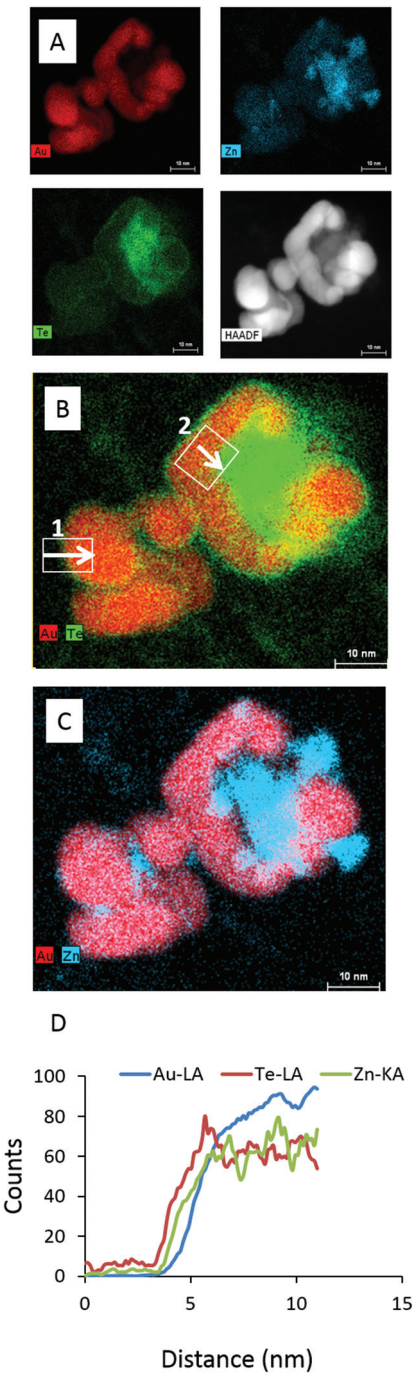

Fig. 2 Elemental analysis of Au–ZnTe core–shell nanoparticles. (A) The presence of Au, Zn and Te in the sample. (B–C) Regions of core–shell and ZnTe nanoparticles. (C) Line scans for the elemental components of Au–ZnTe particles.

when compared to the absorption of the gold at 519 nm. The absorption of ZnTe was observed at 268 nm (Fig. 3B). The photoluminescence spectra of the Au–ZnTe nanoparticles revealed distinct, Gaussian-shaped emission peaks at 402 nm. The crystalline properties of the particles were established by X-ray diffraction analysis; the data confirmed that the core–shell product displayed crystalline features attributable to parental cubic-structured Au and ZnTe (Fig. 3C).

Furthermore, the surface chemistry of the Au–ZnTe nanoparticles was studied using zeta potential analysis to establish their surface charge and to determine how efficiently the coating agent had passivated their outermost surface. The Au and ZnTe parent nanoparticles displayed negative charges of −65.1 mV and −11.7 mV, respectively. The combined core–shell particles showed a positive charge of 0.0519 mV, close to neutral. The outer capping material of cysteine carried a positive charge of 3.95 mV. Thus, cysteine efficiently passivated the surface charge of the Au–ZnTe particles.

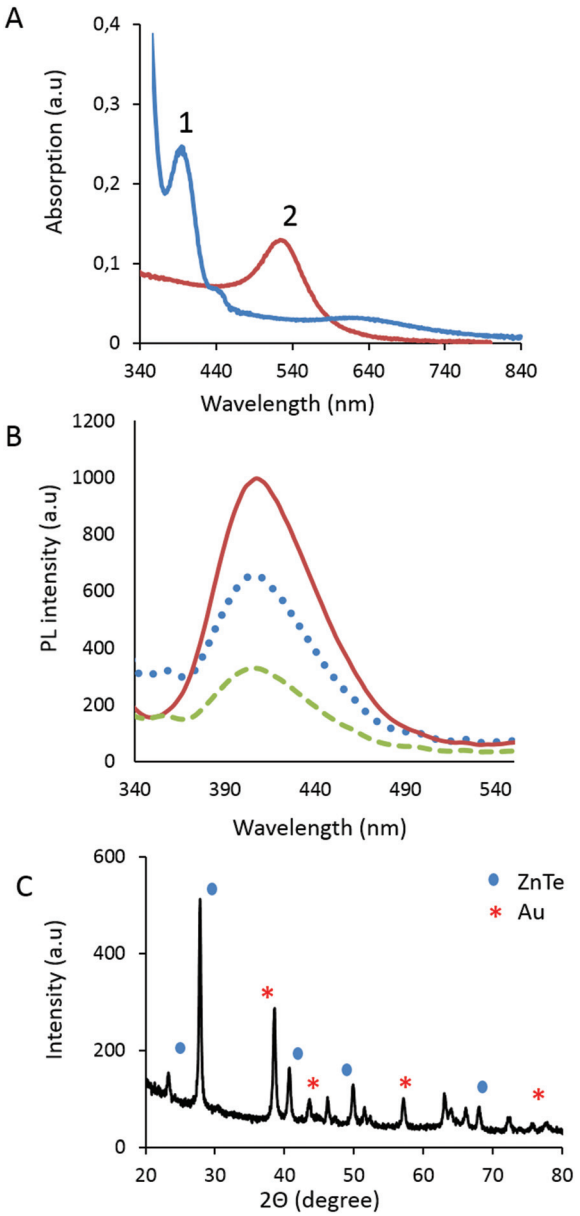

Fig. 3 Optical and crystalline properties of Au–ZnTe core–shell nanoparticles. (A) Displays the UV absorption range for ZnTe and Au–ZnTe nanoparticles. (B) Displays a constant PL emission maxima at 400 nm observed at different excitation wavelengths (1: 300 nm; 2: 310 nm; 3: 315 nm). (C) Displays the XRD pattern for Au–ZnTe core–shell nanoparticles.

Cytotoxicity of Au–ZnTe core–shell nanoparticles using WST-1 assay

The cytotoxicity of Au–ZnTe nanoparticles was established using the WST-1 assay, which is based on the cleavage of a water-soluble tetrazolium salt to a formazan dye by succinate–tetrazolium reductase; this reaction occurs in the mitochondrial respiratory chain and is active only in viable cells. HT29, MCF7 and PC3 cells, as well as CCD 841 CoN and MCF12A cells (Fig. 4) showed no adverse effects on cellular growth during exposure to the nanoparticles; furthermore, the treated cells displayed relative growth that was statistically insignificant ($p > 0.05$) when compared to the controls. Additionally, no significant morphological changes, depicting apoptosis or necrosis, were observed across the different cell types during their co-culture exposure to the Au–ZnTe nanoparticles.

Nanoparticle interference with WST-1 and alamar blue

Au–ZnTe nanoparticles were evaluated for their interaction with WST-1 and alamar blue assay with and without the presence of cells. The results indicated that Au–ZnTe nanoparticles did not influence or cause any statistically significant changes ($p > 0.05$) in absorption of the test reagent nor did the nanoparticle display a catalytic ability to convert WST-1 and alamar blue into its reduced form. Results available in the ESI.†

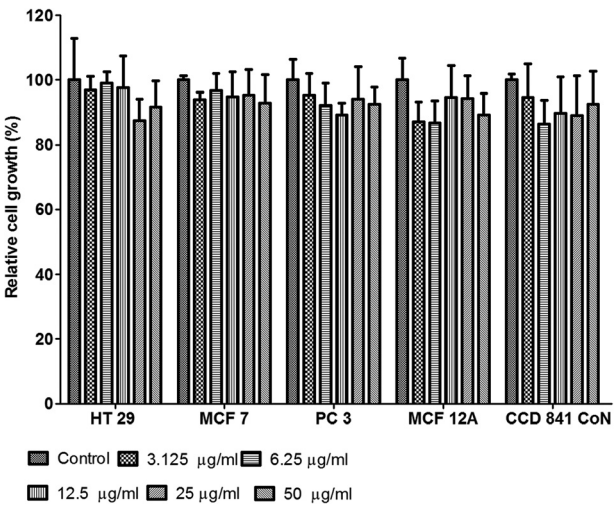

Fig. 4 Cytotoxicity of Au–ZnTe core–shell nanoparticles. The bars display the relative growth of HT29, MCF7 and PC3 cancer cell lines, as well as of the MCF12A and CCD 841 CoN normal cell lines.

Cellular interaction and biocompatibility studies using MCF7 cells

Pre-exposed MCF7 cancer cells were embedded in resin and sectioned for TEM analysis (Fig. 5A). The treated cell sections displayed bio-interactions of the core–shell along the cellular membrane. The cysteine-capped particles interacted with the cell membrane (Fig. 5B–D) and were found to enter the cells' internal environment through cell-mediated endocytosis. Fig. 5C and D show evidence of cellular uptake of the core-shells. This observation not only confirmed the bio-interaction of the core-shells but also demonstrated the cellular uptake and isolation of these particles within the cells.[13] The use of cysteine as a capping agent appears to play a key role in stabilising the nanomaterial and facilitating its biocompatibility.

Immunotoxicity effects of Au–ZnTe core–shell nanoparticles on human PBMCs

PHA-stimulated and non-stimulated human PBMCs were exposed to various concentrations of Au–ZnTe core–shell nanoparticles (50, 25, 12.5, 6.25, 3.125, 1.5, 0.78, 0.39, 0.19 and 0.09 μg ml^{-1}) for 72 hours to simulate an *in vitro* immune response. The effect of the nanoparticles on these blood peripheral cells was studied using the Alamar blue cell proliferation assay to test cell viability. Exposure to Au–ZnTe nanoparticles at concentrations below 3.125 μg ml^{-1} did not induce a dose-dependent reduction in the cell viability of the PHA-treated and non-stimulated PBMCs. The viability of the cells was moderately low (80–95% viability) compared with their corresponding untreated controls (Fig. 6A). There was a clear dose-dependent reduction in the cell viability of the PHA-stimulated and non-stimulated PBMC cells exposed to 6.25 μg ml^{-1} or higher concentrations of the nanoparticles.

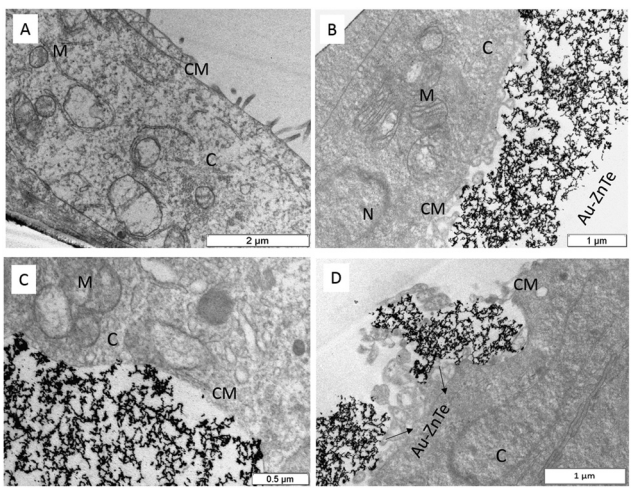

Fig. 5 Biocompatibility of cysteine-capped Au–ZnTe core–shell nanoparticles. (A) Cross section of control MCF7 cells. (B, C) Cross section of MCF7 cells showing Au–ZnTe core–shell nanoparticles aligning along and interacting with the cellular membrane. (D) Evidence of cell-mediated endocytosis of Au–ZnTe core–shell nanoparticles and cellular uptake of the cysteine-capped particles.

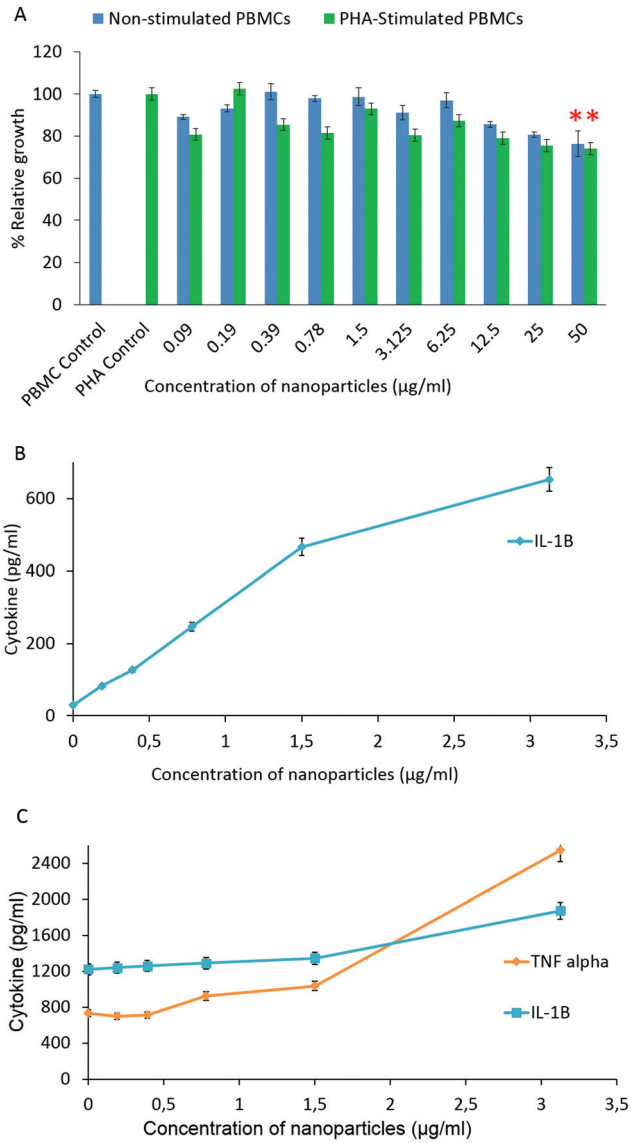

Fig. 6 Immunotoxicity effects of Au–ZnTe core–shell nanoparticles on human peripheral blood mononuclear cells and cytokine expression. (A) Relative growth of PHA-stimulated and non-stimulated PBMCs during co-culture with the nanoparticles. (B) Cytokine expression of non-stimulated PBMCs. (C) Cytokine expression of PHA-stimulated PBMCs. All values are compared to their respective untreated controls, $n = 3$. (*$p < 0.05$).

The nanoparticles at 50 μg ml^{-1} induced 20% reduction in cell viability in both PHA-stimulated and non-stimulated PBMCs, which was statistically significant ($p < 0.05$). Culture media of PHA-stimulated and non-stimulated PBMCs exposed to non-cytotoxic concentrations of Au–ZnTe nanoparticles were evaluated for expression of IFN-γ, IL-1β and TNF-α using commercial ELISA kits. In the non-stimulated PBMCs, the nanoparticles induced a dose-dependent increase in IL-1β expression. The highest nanoparticle concentration tested, 3.125 μg ml^{-1}, induced 643 pg per ml of IL-1β (Fig. 6B). In the PHA-stimulated PBMCs, the Au–ZnTe core–shell nanoparticles

induced a dose-dependent increase in both TNF-α and IL-1β secretion (Fig. 6C). Au–ZnTe core–shell nanoparticles did not induce detectable levels of IFN-γ in either PHA-stimulated or non-stimulated PBMCs.

Effects of Au–ZnTe core–shell nanoparticles on full blood counts in rat models

During the experiments, each animal maintained normal alertness and activity as well as grooming and eating patterns. The animals were handled with care and all procedures were performed under the care of the institutional veterinarian. Blood collected from the rats after acute exposure to Au–ZnTe nanoparticles was analysed to detect abnormalities or changes in blood composition. The accepted rat hematological reference range for RBCs and WBCs is 6.76–9.75 × 10^6 mm^{-3} and 6.6–12.6 × 10^3 mm^{-3}, respectively. Blood platelets were analysed using a reference range of 150–460 × 10^3 ml^{-1}. No statistically significant changes ($p > 0.05$) were observed in the hematological parameters measured across the untreated control and nanoparticle-treated samples (Fig. 7).

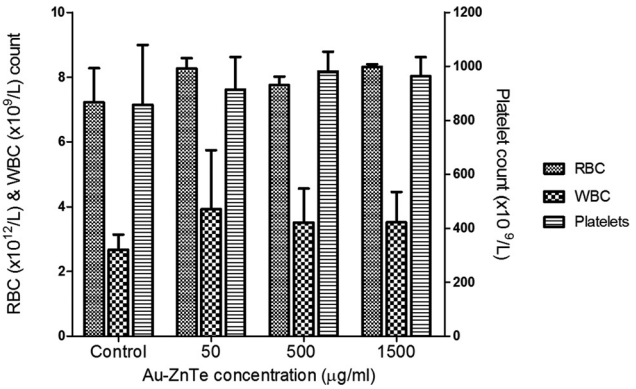

Fig. 7 Hematological analysis of animals treated with Au–ZnTe core–shell nanoparticles. Red, white and platelet blood cells were evaluated. All values are compared to the untreated control, $n = 3$.

Effects of Au–ZnTe core–shell nanoparticles on liver and kidney function in rat models

The biochemical parameters included measures of liver and kidney functions due to their central role in detoxification and excretion (Fig. 8A and B). Serum levels of liver enzymes referenced within the following ranges were measured: ALT: 17.5–30.2 IU l^{-1}, ALP: 56.8–128 IU l^{-1}, gamma-GT: >60 IU l^{-1}, and LDH: 100–250 IU l^{-1}. The results showed no statistically significant ($p > 0.05$) changes across the untreated control and nanoparticles-treated animals (Fig. 6A). Creatine and urea serum levels indicated no statistically significant ($p > 0.05$) changes in the kidney function from animals in the untreated and treated groups (Fig. 6B). The 24 hour urine analysis of all 12 animals displayed no significant differences across the untreated and treated animals. The urine pH was observed at 6.8. The presence of glucose, ketones, bilirubin, blood or haemoglobin appeared negative on the urine dipstick test.

Histological effects of Au–ZnTe core–shell nanoparticles on liver and kidney organs in Sprague Dawley rats

Histology studies were performed on freshly harvested kidney and liver tissue from the experimental rats. The H&E images obtained from the control samples (Fig. 9A) closely resembled the expected morphology of normal healthy renal tissue. The H&E-stained micrographs of the treated samples were all similar to those of the controls, displaying normal tissue morphology and cellular arrangement. Micrographs of the high-dose samples showed no sign of tissue damage or any lesions being present in the entirety of tissue at low magnification (Fig. 9B).

At a higher magnification (Fig. 9C), which allows for a closer inspection of the functional units of the kidney, there appears to be no damage to the Bowman's capsule nor to the

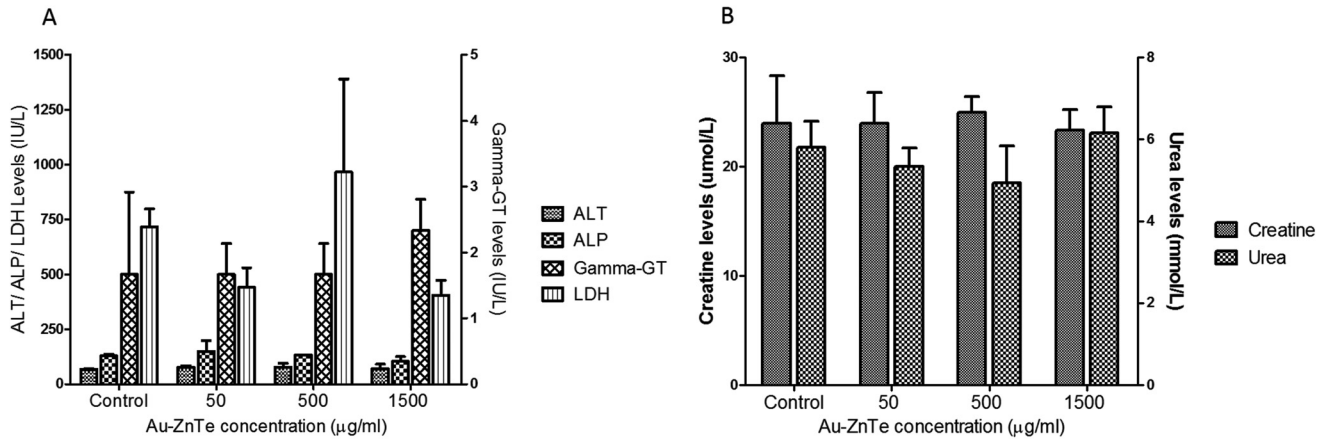

Fig. 8 Effects of Au–ZnTe core–shell nanoparticles on liver and kidney function in Sprague Dawley rats. (A) Liver function tests, showing concentrations of ALT, ALP, gamma-GT and LDH. (B) Kidney function tests, showing concentrations of creatine and urea. All values are compared to their respective untreated control, $n = 3$.

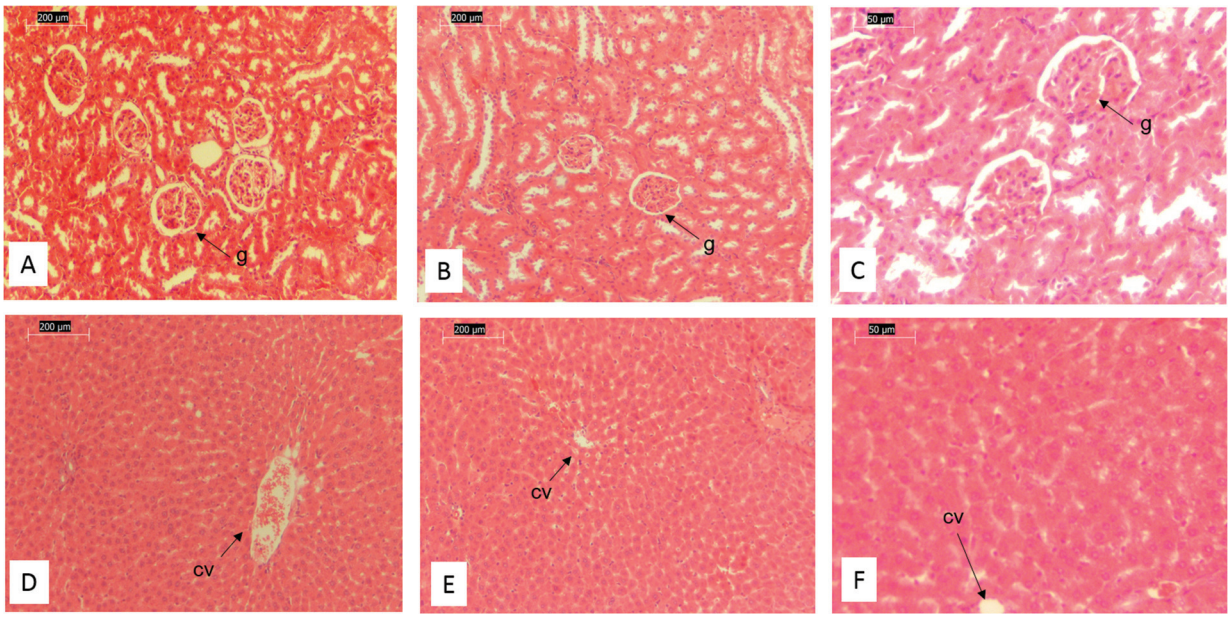

Fig. 9 Histological effects of Au–ZnTe core–shell nanoparticles on liver and kidney organs in Sprague Dawley rats. (A) Tissue section from the untreated control kidney: 10×. (B) Low-magnification micrograph of kidney tissue from a high dose (1500 µg ml^{-1}) treated animal: 10×. (C) High-magnification micrograph of kidney tissue from a high dose (1500 µg ml^{-1}) treated animal: 20×. (D) Tissue section from the untreated control liver: 10×. (E) Low-magnification micrograph of liver tissue from a high dose (1500 µg ml^{-1}) treated animal: 10×. (F) High-magnification micrograph of liver tissue from a high dose (1500 µg ml^{-1}) treated animal: 20×. (g, glomerulus; cv, central vein.)

glomerulus in the treated samples. H&E images of the control sample (Fig. 9D) closely resembled those of normal liver morphology. The images obtained from all the treated samples were similar to those of the controls. At low magnification of the treated samples (Fig. 9E), there were no observable tissue lesions, and at higher magnification (Fig. 9F) the morphology of the hepatocytes appeared to be normal, and similar to that of the controls. These LM images show no loss of cellular integrity within the samples studied.

Discussion

The objective of this study was to synthesize, characterise and evaluate the biosafety of Au–ZnTe core–shell nanoparticles under *in vitro* and *in vivo* experimental conditions. In order to explore the biological potential of this material, an understanding of the bio-interactions across many cell lines is required. In general cytotoxicity and biosafety evaluations of novel materials can be assessed using any eukaryotic cell line, as the basal cell physiology functions remain similar across any cell type. We therefore used five cell lines from different organs to evaluate any changes in cytotoxicity responses to our nanomaterials across the cell types. The outcome was that the particles displayed no adverse effects on cellular proliferation of CCD 841 CoN, MCF12A, MCF7, HT29 and PC3 cells at the concentrations tested.

Moreover, normal breast epithelial and colon cells grown under co-culture exposure to Au–ZnTe nanoparticles showed no cytotoxic effects from bio-interactions. The absorption peak of Au–ZnTe nanoparticles is 538 nm (Fig. 3) with an active absorbance wavelength range between 460–580 nm. In general it is observed that nanoparticle interference with biochemical assays which are based on the photometric principle will not be affected if the selected wavelength does not overlap the active absorption range of nanoparticles.[30] Work reported by Dobrovolskaia and co-workers demonstrated this concept using the overlapping absorbance spectrums of gold nanoparticles and the classical hemolysis assay.[31] Optical, catalytic and surface properties of nanomaterials play a key role in cytotoxicity data interference and observable artifacts. It is therefore necessary to develop screening techniques and appropriate controls to validate photometric biochemical assays. In an independent study, dose-dependent toxicity of nanoparticles was observed on renal cell lines; this study demonstrated the effect of size and concentration of such materials on renal cell function. The literature highlights the importance of standardizing *in vitro* cellular systems for nanotoxicity and biosafety screening and in establishing a safe dose/concentration range that could be used for bio-applications.[13,24,25,28,29,32,33] An important aspect of biosafety of nanomaterials is related to their size, shape and composition.

Some reported studies have demonstrated that exposure to larger nanoparticles triggers macrophage responses that activate the immune system.[31] In our study, human peripheral blood mononuclear cells were used to simulate an *in vitro* immune system. The protein phytohemagglutinin (PHA) is a molecule that is used as a mitogen to trigger T-lymphocyte cell

division and to activate growth of human peripheral lymphocytes.[34] The function of PHA stimulation is to mimic an active immune system that is stimulated to produce more active mononuclear cells, whereas the PBMCs that grow at their normal rate or are unstimulated represent an inactive immune system. The effects of Au–ZnTe nanoparticles on both active and inactive immune systems showed a 20% decrease in cell viability at 50 μg ml^{-1}. Paino *et al.*[35] reported the cytotoxic effects of sodium citrate and polyamidoamine-capped gold nanoparticles on human PBMCs in a dose-dependent manner. The results also confirmed that immune cells are less sensitive to DNA damage than cancer HepG2 cells. Cellular responses during exposure to, or co-culture with, nanomaterials are interpreted based on what is observed; however, the thousands of cell cycle events that take place regardless of our observation may well be the missing link to enable scientists to monitor cellular immune functions.[34,35]

The effects of Au–ZnTe nanoparticles were further evaluated by investigating the expression of cell signaling proteins called cytokines. The serum from both PHA-stimulated and non-stimulated PBMCs were evaluated for expression of IFN-γ, IL-1β and TNF-α. IL-1β and TNF-α were expressed in very small amounts relative to the concentration of the nanoparticles, indicating the immunomodulatory effects of the particles and the presence of a systematic functional immune system at the *in vitro* level. These results clearly indicate that accumulation of high concentrations of Au–ZnTe nanoparticles within biological systems may trigger immune responses through the dose-dependent increased expression of these cytokines.

The use of animals in laboratory research allows for biosafety evaluations across integrated organ systems and whole animal studies, providing more information on short- and long-term immune responses, enzyme function, cellular responses, cytotoxicity and genotoxicity. The acute toxicity effects and bio-interaction studies of Au–ZnTe nanoparticles were tested on Sprague Dawley rats over an exposure of 7 days.

Literature often highlights the importance of maintaining vital cellular and enzyme functions so that homeostasis is not interrupted through the interaction of nanoparticles.[13,32–39] In the blood circulatory system, red blood cells function in gaseous exchange, white blood cells provide immune protection whereas platelets initiate coagulation of blood.[13,29] In addition the enzymes produced in the liver and kidney organs provide vital roles in detoxification and excretion physiology. ALT catalyses the transfer of an amino group from L-alanine to α-ketoglutarate, leading to the production of pyruvate and L-glutamate. ALP is responsible for dephosphorylating biomolecules. Gamma-GT plays a regulatory role at various levels in cellular signal transduction and cellular pathophysiology. Lactate dehydrogenase is found extensively in body tissues and cells. During tissue damage, LDH is released from impaired membranes; this enzyme is used as a marker of common injuries and disease. In the kidney urea serves an important role in the metabolism of nitrogen-containing compounds and the nitrogenous organic acid creatine helps to supply energy to all cells in the body, primarily the muscle through the increased formation of adenosine triphosphate.[34–37] These enzymes and protein molecules function systemically to maintain optimal liver and kidney functions. Evaluations of these parameters provide valuable information on the status of the kidney and liver functions during acute exposure to nanoparticles.

Histomorphological evaluations are vital tools that can be used to assess tissue damage and/or cellular abnormalities after exposure to a treatment regimen. Although limited, LM assessments can provide insight into the potential disruptions at the tissue level, thereby inferring change in functionality of the organ system. The functional unit of the kidney is the nephron, which comprises the Bowman's capsule and the glomerulus. Our LM observations showed no significant changes in the treated samples, which therefore suggests that there was no loss of kidney function in the treated groups as compared to the control. This notion was further confirmed by the data obtained for the renal functionality tests (Fig. 8B) that displayed no significant differences between the measurements for creatine and urea levels between the control and experimental animals.

The liver comprises many lobules which make up its functional unit. Each lobule contains millions of hepatocytes which are the basic metabolic cells of the organ. Assessments of the treated samples showed no change in the morphology of the hepatocytes, which therefore indicates similar functionality of the liver in both the treated and control animals. Interestingly, the data obtained for the ALT, ALT Phos, gamma-GT and LDH levels (Fig. 8A) from the liver functionality tests displayed no significant differences between control and treated groups, which directly correlates with inferences made from the histological evaluations. We therefore deduce that these organ systems suffered no toxic effects after exposure to Au–ZnTe nanoparticles for seven days. Furthermore, throughout the experimental period, no changes in behaviour or other unusual responses were observed in the animals treated with low, intermediate and high doses of Au–ZnTe nanoparticles. The full blood count measurements indicated no significant changes across the control and nanoparticle-treated rats. The normal levels of white blood cells in the rat can be correlated with the relative growth of PBMCs in the *in vitro* experiment. In both cases Au–ZnTe nanoparticles showed no adverse effects on immune cells. In addition the liver and kidney enzymes from the treated rats showed no significant differences compared with the control animals. Lee *et al.* described the biopersistence effects on Sprague Dawley rats of exposure to silver nanoparticles.[39] Their results confirmed that the size of the silver nanoparticles did not affect tissue distribution and other hematogical parameters, although the exposure to these nanoparticles did indicate moderate liver abnormalities. In another study silver nanoparticles and silver acetate were administered to rats over 28 days. This study showed that 63% of the silver nanoparticles were expelled in the excrement.[40]

In our study the liver and kidney tissues showed no signs of tissue damage or visible lesions. Magaye *et al.* also used Sprague Dawley rats to establish acute toxicity of nickel nanoparticles; their results revealed no significant changes in red

or white blood cell counts. In addition there were no significant histopathological changes in tissue sections from the rat lung, liver and spleen.[41] These findings suggest that increased exposure times and concentration of nanoparticles during short-term animal studies play an important role in assessing *in vivo* biosafety of nanomaterials.

Conclusions

The *in vitro* and *in vivo* biosafety of Au–ZnTe core–shell nanoparticles was established through the use of various human cells and Sprague Dawley rats. The study provided important information on cellular and organ interactions and on the systemic circulation of these nanoparticles. Our future research aims to understand the degradation and elimination effects of bio-accumulated Au–ZnTe nanoparticles. Overall, the present study successfully demonstrated the biosafety and biocompatibility of these core–shell nanoparticles and sets the platform for future applications in drug delivery and bio-imaging through the use of surface modifications.

Conflict of interest

The authors declare no conflict of interest. No benefit of any kind will be received either directly or indirectly by the authors.

Acknowledgements

We thank the University of Zululand and the Biomedical Resource Unit of the University of KwaZulu-Natal, for technical services and support. Edward. A. Lewis, Sarah. J. Haigh and Paul O'Brien from the School of Chemistry, University of Manchester are acknowledged for their contribution in performing elemental analysis. This work was supported by the Department of Science and Technology and National Research Foundation of South Africa through the DST/NRF South African Research Chairs Initiative (SARCHi) programme.

Notes and references

1 R. Ghosh Chaudhuri and S. Paria, *Chem. Rev.*, 2011, **112**, 2373–2433.
2 L. Carbone and P. D. Cozzoli, *Nano Today*, 2010, **5**, 449–493.
3 A. Nag, J. Kundu and A. Hazarika, *CrystEngComm*, 2014, **16**, 9391–9407.
4 Q. Tian, J. Hu, Y. Zhu, R. Zou, Z. Chen, S. Yang, R. Li, Q. Su, Y. Han and X. Liu, *J. Am. Chem. Soc.*, 2013, **135**, 8571–8577.
5 J. Wang, K. Zhao, X. Shen, W. Zhang, S. Ji, Y. Song, X. Zhang, R. Rong and X. Wang, *J. Mater. Chem. C*, 2015, **3**, 12418–12429.
6 N. T. Thanh and L. A. Green, *Nano Today*, 2010, **5**, 213–230.
7 Z. Sun, Z. Yang, J. Zhou, M. H. Yeung, W. Ni, H. Wu and J. Wang, *Angew. Chem., Int. Ed.*, 2009, **48**, 2881–2885.
8 D.-K. Lim, I.-J. Kim and J.-M. Nam, *Chem. Commun.*, 2008, 5312–5314.
9 H.-Y. Park, M. J. Schadt, L. Wang, I.-I. S. Lim, P. N. Njoki, S. H. Kim, M.-Y. Jang, J. Luo and C.-J. Zhong, *Langmuir*, 2007, **23**, 9050–9056.
10 S. Kayal and R. V. Ramanujan, *J. Nanosci. Nanotechnol.*, 2010, **10**, 5527–5539.
11 W. J. Stark, *Angew. Chem., Int. Ed.*, 2011, **50**, 1242–1258.
12 N. C. Bigall, W. J. Parak and D. Dorfs, *Nano Today*, 2012, **7**, 282–296.
13 R. Dunpall, E. A. Lewis, S. J. Haigh, P. O'Brien and N. Revaprasadu, *J. Mater. Chem. B*, 2015, **3**, 2826–2833.
14 K. Chatterjee, S. Sarkar, K. J. Rao and S. Paria, *Adv. Colloid Interface Sci.*, 2014, **209**, 8–39.
15 J. Li, X. Chang, X. Chen, Z. Gu, F. Zhao, Z. Chai and Y. Zhao, *Biotechnol. Adv.*, 2014, **32**, 727–743.
16 P. Ghosh, G. Han, M. De, C. K. Kim and V. M. Rotello, *Adv. Drug Delivery Rev.*, 2008, **60**, 1307–1315.
17 S. Kondath, B. S. Raghavan, R. Anantanarayanan and R. Rajaram, *Chem.-Biol. Interact.*, 2014, **224**, 78–88.
18 C. Kirchner, A. M. Javier, A. Susha, A. Rogach, O. Kreft, G. Sukhorukov and W. Parak, *Talanta*, 2005, **67**, 486–491.
19 P. Borm and V. Castranova, *Part. Fibre Toxicol.*, 2009, **6**, 13.
20 K. S. Kumar, V. B. Kumar and P. Paik, *J. Nanopart.*, 2013, **2013**, 672059.
21 W. Cui, J. Li, Y. Zhang, H. Rong, W. Lu and L. Jiang, *Nanomedicine*, 2012, **8**, 46–53.
22 S. K. Sohaebuddin, P. T. Thevenot, D. Baker, J. W. Eaton and L. Tang, *Part. Fibre Toxicol.*, 2010, **7**, 22.
23 B. Sha, W. Gao, S. Wang, F. Xu and T. Lu, *Composites, Part B*, 2011, **42**, 2136–2144.
24 C. Freese, C. Uboldi, M. I. Gibson, R. E. Unger, B. B. Weksler, I. A. Romero, P.-O. Couraud and C. J. Kirkpatrick, *Part. Fibre Toxicol.*, 2012, **9**, 23.
25 A. R. Gliga, S. Skoglund, I. O. Wallinder, B. Fadeel and H. L. Karlsson, *Part. Fibre Toxicol.*, 2014, **11**, 11.
26 Y. Liu, K. Yang, L. Cheng, J. Zhu, X. Ma, H. Xu, Y. Li, L. Guo, H. Gu and Z. Liu, *Nanomedicine*, 2013, **9**, 1077–1088.
27 T. Li, B. Albee, M. Alemayehu, R. Diaz, L. Ingham, S. Kamal, M. Rodriguez and S. W. Bishnoi, *Anal. Bioanal. Chem.*, 2010, **398**, 689–700.
28 P. J. Borm, D. Robbins, S. Haubold, T. Kuhlbusch, H. Fissan, K. Donaldson, R. Schins, V. Stone, W. Kreyling and J. Lademann, *Part. Fibre Toxicol.*, 2006, **3**, 11.
29 G. Oberdörster, A. Maynard, K. Donaldson, V. Castranova, J. Fitzpatrick, K. Ausman, J. Carter, B. Karn, W. Kreyling and D. Lai, *Part. Fibre Toxicol.*, 2005, **2**, 8.
30 K. J. Ong, T. J. MacCormack, R. J. Clark, J. D. Ede, V. A. Ortega, L. C. Felix, M. K. Dang, G. Ma, H. Fenniri and J. G. Veinot, *PLoS One*, 2014, **9**, e90650.
31 M. A. Dobrovolskaia, J. D. Clogston, B. W. Neun, J. B. Hall, A. K. Patri and S. E. McNeil, *Nano Lett.*, 2008, **8**, 2180–2187.

32 B. L'Azou, J. Jorly, D. On, E. Sellier, F. Moisan, J. Fleury-Feith, J. Cambar, P. Brochard and C. Ohayon-Courtès, *Part. Fibre Toxicol.*, 2008, **5**, 651–663.
33 I. Pujalté, I. Passagne, B. Brouillaud, M. Tréguer, E. Durand, C. Ohayon-Courtès and B. L'Azou, *Part. Fibre Toxicol.*, 2011, **8**, 1–16.
34 Z. Vlata, F. Porichis, G. Tzanakakis, A. Tsatsakis and E. Krambovitis, *Toxicol. Lett.*, 2006, **165**, 274–281.
35 I. M. M. Paino, V. S. Marangoni, R. d. C. S. de Oliveira, L. M. G. Antunes and V. Zucolotto, *Toxicol. Lett.*, 2012, **215**, 119–125.
36 S. Y. Shann, C. M. Lau, S. N. Thomas, W. G. Jerome, D. J. Maron, J. H. Dickerson, J. A. Hubbell and T. D. Giorgio, *Int. J. Nanomed.*, 2012, **7**, 799.
37 H. Eidi, O. Joubert, G. Attik, R. Duval, M. Bottin, A. Hamouia, P. Maincent and B. Rihn, *Int. J. Pharm.*, 2010, **396**, 156–165.
38 M. Reddy, E. Eirikis, C. Davis, H. M. Davis and U. Prabhakar, *J. Immunol. Methods*, 2004, **293**, 127–142.
39 J. H. Lee, Y. S. Kim, K. S. Song, H. R. Ryu, J. H. Sung, J. D. Park, H. M. Park, N. W. Song, B. S. Shin and D. Marshak, *Part. Fibre Toxicol.*, 2013, **10**, 16968–16973.
40 K. Loeschner, N. Hadrup, K. Qvortrup, A. Larsen, X. Gao, U. Vogel, A. Mortensen, H. R. Lam and E. H. Larsen, *Part. Fibre Toxicol.*, 2011, **8**, 18.
41 R. R. Magaye, X. Yue, B. Zou, H. Shi, H. Yu, K. Liu, X. Lin, J. Xu, C. Yang and A. Wu, *Int. J. Nanomed.*, 2014, **9**, 1393.